

This article may be downloaded for personal use only. Any other use requires prior permission of the author and AIP Publishing. This article appeared in C. Teodorescu, R. Clary, R. F. Ellis, A. B. Hassam, C. A. Romero-Talamas, W. C. Young; Sub-Alfvénic velocity limits in magnetohydrodynamic rotating plasmas. Phys. Plasmas 1 May 2010; 17 (5): 052503. <https://doi.org/10.1063/1.3383051> and may be found at <https://pubs.aip.org/aip/pop/article-abstract/17/5/052503/920544/Sub-Alfvenic-velocity-limits-in?redirectedFrom=fulltext>.

Access to this work was provided by the University of Maryland, Baltimore County (UMBC) ScholarWorks@UMBC digital repository on the Maryland Shared Open Access (MD-SOAR) platform.

Please provide feedback

Please support the ScholarWorks@UMBC repository by emailing scholarworks-group@umbc.edu and telling us what having access to this work means to you and why it's important to you. Thank you.

RESEARCH ARTICLE | MAY 14 2010

Sub-Alfvénic velocity limits in magnetohydrodynamic rotating plasmas

C. Teodorescu; R. Clary; R. F. Ellis; A. B. Hassam; C. A. Romero-Talamas; W. C. Young



Phys. Plasmas 17, 052503 (2010)

<https://doi.org/10.1063/1.3383051>



CrossMark



AIP Advances

Why Publish With Us?

**25 DAYS**
average time
to 1st decision

**740+ DOWNLOADS**
average per article

**INCLUSIVE**
scope

[Learn More](#)

 AIP
Publishing

Sub-Alfvénic velocity limits in magnetohydrodynamic rotating plasmas

C. Teodorescu, R. Clary, R. F. Ellis, A. B. Hassam,
C. A. Romero-Talamas, and W. C. Young
University of Maryland, College Park, Maryland 20742, USA

(Received 15 December 2009; accepted 17 March 2010; published online 14 May 2010)

Magnetized plasmas in shaped fields rely on large, supersonic rotation to effect centrifugal confinement of plasma along magnetic field lines. The results of experiments on the Maryland Centrifugal Experiment (MCX) [R. F. Ellis *et al.*, Phys. Plasmas **12**, 055704 (2005)] to document velocity limits are reported. Previous results have shown a limit at the Alfvén speed, consistent with equilibrium limits from ideal magnetohydrodynamic theory. Another speed limit, previously reported as possibly related to a critical ionization phenomenon and depending only on the ion species and the shape of the confining magnetic field, is investigated here for a broad range of the applied parameters. We show that this speed limit manifests at sub-Alfvénic levels and that, as externally applied torques on the plasma are increased, the extra momentum input shows up as enhanced plasma density or lower momentum confinement time, accompanied by an increase in the neutral radiation level. Several key parameters are scanned, including the mirror ratio, the length between insulators, and the species mass. We show that this velocity limit is consistent with the species-dependent critical ionization velocity postulated by Alfvén. © 2010 American Institute of Physics. [doi:10.1063/1.3383051]

I. INTRODUCTION

Magnetized, centrifugally confined, rotating plasmas constitute a possible configuration for containing plasmas for thermonuclear fusion, where inertial forces from rotation augment the conventional magnetic confinement. Fusion performance in this system can be maximized when the azimuthal flow is larger than the ion thermal speed, i.e., supersonic flow.¹ High sonic Mach number ($M_s = u_\phi / v_{th}$, where u_ϕ is the flow speed and v_{th} is the thermal speed) flow is the theoretical figure of merit to achieve strong axial centrifugal confinement, robust magnetohydrodynamic (MHD) stability, and minimal axial electron energy heat losses. The flow speed must, however, be sub-Alfvénic, as, if the flow speed approaches the Alfvén speed, a bowing out of the magnetic mirror field results, degrading the confinement and the equilibrium. This operational upper bound at the Alfvén Mach number $M_A \equiv u_\phi / v_A$, where $v_A = B / (\mu_0 \rho)^{1/2}$, of the order of unity has already been documented in the magnetized rotating plasma produced in Maryland Centrifugal Experiment (MCX).²

Another limit on the plasma rotation has been widely reported in previous experiments on magnetized and non-magnetized rotating plasmas. This limit has been the focus of two extensive review works by Brenning³ and by Lai,⁴ which describe almost 150 laboratory and space experiments spanning over 45 yr, in which the voltage across the plasma, and hence the plasma rotation speed, seems to be capped for increasing external torque applied on the plasma. The velocity limitation observed in these experiments has been attributed to the manifestation of the critical ionization velocity (CIV) phenomenon, first proposed by Alfvén⁵ to explain features in solar wind flow: as the ion flow kinetic energy exceeds the ionization potential of the species in question, an enhanced ionization occurs in the plasma-neutral interaction

layer, in turn, placing a drag on the plasma rotation as energy from the rotating ions is transferred to the ionizing neutrals and as the mass load increases from increasing density. The neutral gas becomes ionized when the relative velocity between the gas and the plasma ions reaches the critical value $v_{crit} = (2e\varphi_i/m)^{1/2}$, where φ_i is the ionization potential of the atom, m is the mass of the ion in motion, and e is the absolute value of the electron charge. For protons streaming through hydrogen neutrals, $v_{crit} = 51.4$ km/s. Thus, the CIV is only species dependent, depending only on the species mass and ionization potential.

This work reports on the systematic investigation to ascertain the speed limitation in MCX when plasma is away from the “Alfvén Mach number limit” $M_A \leq 1$. The available range in the MCX external parameters is used to increase the voltage across the plasma and hence the rotation speed: the key parameters that are scanned include the mirror ratio, the length between insulators, and the species mass. There is also another external parameter, an external series resistor R_s (described in more detail later), that is also scanned: this is related to the fact that the voltage across the plasma cannot simply be set externally since, for a given applied external voltage, the voltage drop across the plasma depends on the plasma internal resistance. The latter is not under direct experimental control, depending, as it does, on the transport confinement quality of the plasma. Thus, by changing the value of an external resistor that is placed in series in the circuit, one may attempt to place varying voltage on the plasma, at least initially. This work also takes into account confinement times and exploits the variability of the external resistor.

Previous laboratory experiments in MHD rotating plasmas for fusion aimed at studying the velocity limit were performed from the 1960s until the late 1980s. They were

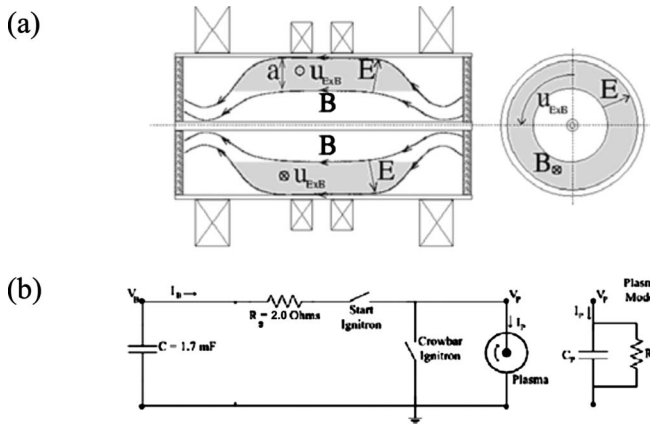


FIG. 1. (a) Schematic of MCX (the total length is 4 m). Here, $u_{E \times B} \equiv u_\phi$. (b) External circuitry of MCX.

started by Fahleson⁶ and continued by Angerth *et al.*⁷ in a homopolar device (with uniform axial magnetic field). The first experiments in an inhomogeneous (i.e., shaped) magnetic field were performed in 1966 by Bergstrom *et al.*,⁸ Lehnert,⁹ and Lehnert *et al.*,¹⁰ and continued with the work of Danielsson,¹¹ Piel *et al.*,¹² and Brenning.¹³ The latest work on the velocity limits of rotating plasma contained in a shaped magnetic field were performed by Abdrashitov *et al.*¹⁴ Although these early experiments were made in devices similar to MCX in the sense that plasma rotation was a “knob” for controlling the confinement, MCX is different than those experiments in terms of having almost one order of magnitude larger confinement time, operating at a larger mirror ratio, and being able to distinguish between the CIV and the Alfvén Mach number limit by measuring directly both the rotation speed and the Alfvén speed. With the exception of Abdrashitov *et al.*,¹⁴ the other experiments do not measure plasma density when the velocity caps off, thus they cannot distinguish easily which of the two limits applies, leading to uncertainty in the results.

II. APPARATUS

MCX is a modified mirror machine [mirror ratio $R_m = B_z(z=1.3 \text{ m})/B_z(z=0)$ between 1 and 19], in which a central metallic core that runs axially through the vessel serves as the high voltage electrode, which is biased negatively with respect to the grounded vessel using an ignitron switched capacitor bank of 1.8 mF (Fig. 1). Insulating disks (using a grooved Macor piece of 0.2 m in diameter and a Pyrex piece of 0.45 m in diameter tied together)² placed usually but not necessarily at the mirror throats ($z=1.3 \text{ m}$ and $z=-1.3 \text{ m}$, respectively, from the midplane) limit the plasma in the axial direction and ensure that the magnetic field lines are also equipotential lines. When $R_m=8$, the plasma is radially limited by the conductive core, which defines the inner last-good-flux-surface (LGFS) with radius of $r_1=0.06 \text{ m}$ at the midplane, and by the grounded vessel, which defines the outer LGFS with radius of $r_2=0.26 \text{ m}$ at the midplane. The working gas is hydrogen, which usually uniformly prefills the chamber. A current-limiting resistor R_s

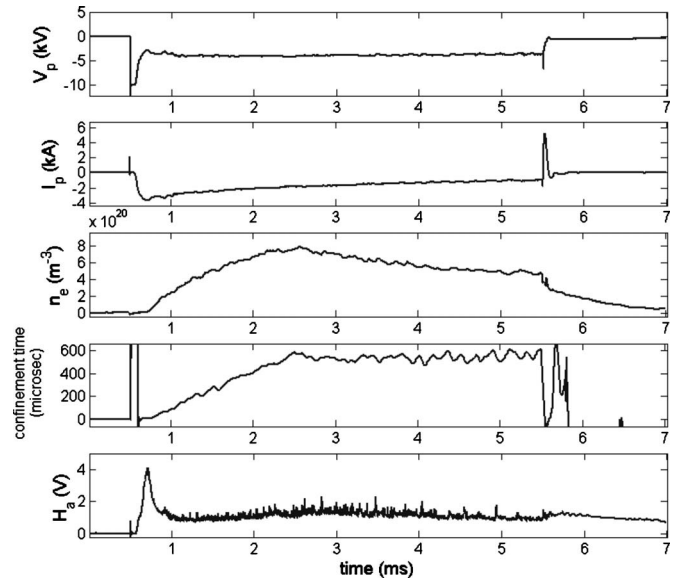


FIG. 2. Plasma voltage, plasma current, line-integrated plasma density at the midplane, momentum confinement time, and H_α signal at the midplane when $V_{\text{bank}}=-10 \text{ kV}$, $B=0.23 \text{ T}$, $R_m=7.5$, $R_s=2 \text{ }\Omega$, and $p=5 \text{ mTorr}$. The plasma is initiated at $t=0.5 \text{ ms}$ and terminated at $t=5.5 \text{ ms}$.

is in series with the capacitor bank. The purpose of this resistor is to control the voltage across the plasma.

Plasma breakdown is thus created in an $\mathbf{E} \times \mathbf{B}$ configuration. The fully ionized, azimuthally rotating plasma lasts for as long as the bank voltage is substantial. The plasma can be terminated after a predetermined time (usually up to 10 ms) by disconnecting it from the capacitor bank, or by short-circuiting it to ground using a fast “crowbar” ignitron. In the latter instance, a large current reversal is measured as the plasma dumps the stored charge and reduces its speed. Relevant diagnostics include a voltage divider, Rogowski coil, multichord Turner–Czerny spectrometer, an interferometer, and several light detectors tuned to the H_α wavelength. Typical signals of plasma voltage, plasma current, plasma density, and magnetic flux variations are shown in Fig. 2. The data reported in this paper are based on a campaign conducted on MCX between May 5, 2007 and February 9, 2009. With the exception of the interferometer, the location of the diagnostics can be set outside the vacuum vessel according to the specific needs of each experiment performed.

Under all the applied parameters, MCX plasma rotation is dominated by the $\mathbf{E} \times \mathbf{B}$ drift and the rotation velocity is $u_\phi = E/B$.^{2,15} Spectroscopy measurements yield information on the ion temperature based on the Doppler broadening of the spectral lines, a typical number being $T_i = 40 \pm 10 \text{ eV}$. By comparing the relative intensity of spectral lines, an upper bound of the electron temperature was found at $T_e = 10 \text{ eV}$.¹⁶ An important plasma parameter is the plasma momentum confinement time τ . This can be calculated using a simple zero-dimensional (0-D) model.¹⁷ As evident from the equivalent circuit shown in Fig. 1, the “free-wheeling” spin-down time of the plasma is due to the plasma resistance R_p and so given as $\tau = R_p C_p$, where C_p is the plasma capacitance. Assuming quasisteady state, this can be recast as

$$\tau = R_p C_p \equiv \frac{V_p}{I_p} C_p = \frac{Q_p}{I_p}, \quad (1)$$

i.e., the confinement time is the time taken for the excess charge in the capacitor to be neutralized by the crossfield current. Both the stored charge and the plasma current I_p are measured experimentally, yielding the confinement time. This simple definition, tested and confirmed earlier,¹⁸ will be utilized in the present paper.

Since MCX is a pulsed experiment, the question of discharge-to-discharge reproducibility arises. It has been documented² that the discharges under the same external parameters are similar within 10%. It can also be seen from the circuit diagram of Fig. 1 that for an approximately time-constant applied bank voltage, the steady-state plasma voltage V_p is a fraction of the bank voltage,

$$V_p = \frac{V_{\text{bank}}}{1 + \frac{R_s}{R_p}}. \quad (2)$$

Thus, by adjusting the series resistance and bank voltage appropriately, the same voltage can appear across the plasma. Ideally, this should be the case even though the plasma resistance is not constant and depends on the voltage across it. This reproducibility check has also been documented.² The results showed that for different values of V_{bank} and R_s , plasma parameters do not change irrespective of the actual values of V_{bank} and R_s . R_s is thus an additional control parameter to change voltage across the plasma. Its limitations will be discussed later.

III. EXPERIMENTS

In a previous work,² the available range of the applied parameters were swept in equal increments: five steps in the case of the bank voltage (from -5 to -17 kV) and fill pressure (from 0.5 to 10 mTorr), six steps in the case of magnetic field (0.08 to 0.23 T), hence obtaining a parameter matrix of 150 elements. The plasma rotation velocity was documented to stay below the Alfvén velocity v_A for the entire range of the applied parameters. This is the so-called Alfvén Mach number limit, which is expressed by $M_A \leq 1$ and it is shown in Fig. 3 (reproduced from Ref. 2) as the accumulation of data points below the oblique line of equation $u_\phi = v_A$.

Those experiments have also shown that for a fixed mirror ratio $R_m = B_z(z=1.3 \text{ m})/B_z(z=0)$ of 7.3 and a fixed value of the series resistor $R_s = 2 \text{ } \Omega$, the plasma rotation velocities attained did not exceed 139 km/s. This limit was different than the Alfvén Mach number limit in the sense that no data points accumulation below the line of equation $u_\phi = 139 \text{ km/s}$ were observed and $M_A \ll 1$.

It has also been shown² that, under conditions where $v_A > 139 \text{ km/s}$, the plasma momentum confinement time decreases as u_ϕ approaches 139 km/s, suggesting the presence of some mechanism that increases the momentum loss as the plasma speed is increased toward that value. The criterion used in selecting the peak value of the voltage was that the value must be maintained over a period of time greater than or commensurate with the plasma confinement time.

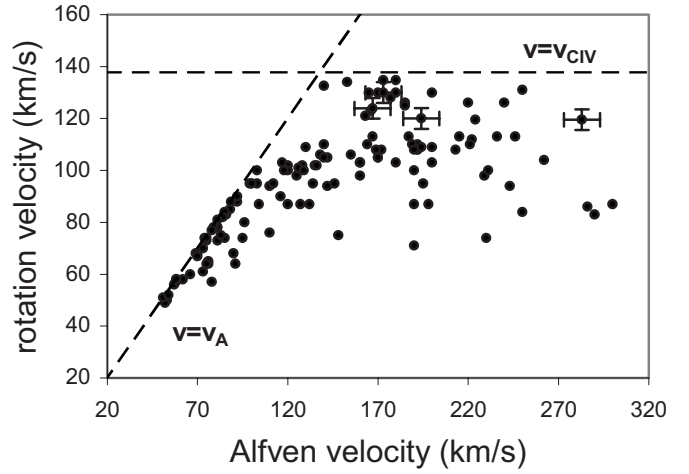


FIG. 3. Plasma rotation velocity and the corresponding Alfvén velocity for 150 discharges obtained with the available range of the applied parameters.

(For instance, for traces shown in Fig. 2, the maximum absolute value of the plasma voltage is 4.9 kV.) Thus, any very short transients were eliminated.

The current experiments are aimed at documenting further whether velocities above 139 km/s (in a mirror configuration of $R_m = 7.3$ or else) could be attained and whether a decrease in the confinement as u_ϕ increases toward 139 km/s could be avoided.

A. Parameter scans and trend of rotation velocity

Parameter scans were performed by varying one external parameter (applied voltage, magnetic field, series resistor, or mirror ratio), while maintaining the other parameters at such values which provide otherwise maximum plasma rotation and confinement time. Assuming plasma isorotation¹⁹ [which means that the angular velocity $\Omega \equiv d\phi/dt$, where ϕ is the angular displacement, is effectively $\Omega(\psi) \equiv dV_p/d\psi$, in other words, angular velocity is the same along a magnetic flux contour], the plasma rotation velocity, as measured at the midplane, can be mapped to the insulator location. Using the magnetic flux conservation, the mapping is described by the equation

$$u_{\phi}^{\text{midplane}} = u_{\phi}^{\text{insulator}} \times R_m^{1/2}. \quad (3)$$

In what follows, this mapping will be used, when appropriate, for comparisons with theory.

The applied voltage was scanned from -6 to -17 kV, while keeping the magnetic field at the maximum value (0.22 T) for the mirror ratio of $R_m = 7.5$ using $R_s = 2 \text{ } \Omega$. The results of these scans are shown in Fig. 4. Here, the measured velocity stays below 118 km/s and caps off as the applied voltage is increased. For all these data points, the condition $v_A > 140 \text{ km/s}$ was measured experimentally.

For a fixed mirror ratio of $R_m = 7.5$, and using first -10 kV and then -17 kV as the applied voltage, increasing the magnetic field leads to an increase in the plasma rotation velocity, as seen in Fig. 5. Although the trend is similar to that shown in Fig. 4, the main difference is in the absence of saturation in the data points below a certain velocity. For all

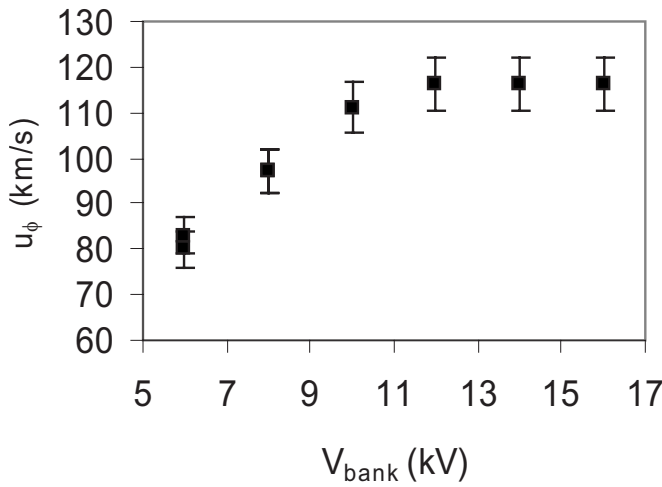


FIG. 4. Dependency of plasma rotation velocity at the midplane on the absolute value of the applied voltage for $B=0.23$ T, $R_m=7.5$, $R_s=2$ Ω , and $p=5$ mTorr.

these data points, the condition $v_A > 140$ km/s was measured experimentally. Judging from the increasing trend of u_ϕ , it might be inferred that higher B operation could result in speeds greater than 120 km/s (improvement in confinement time is expected). However, the rate of increase in speed is relatively low, i.e., $\Delta u_\phi / \Delta B \approx 200$ km/(s T) between 0.15 T $< B < 0.25$ T: to reach the Alfvén velocity (in the 200 km/s range) would require an extrapolation in B to 0.75 T.

A scan where all parameters are kept the same except for the series resistor was also performed. Reducing R_s would tend to increase plasma current I_p ; if plasma resistance R_p stayed the same, this would place a larger voltage V_p across the plasma. In Fig. 6, the mirror ratio is 7, the magnetic field at the midplane is 0.21 T, and the applied voltage is -10 kV. It can be seen that plasma rotation reaches a maximum of about 130 km/s for $R_s=0.5$ Ω and has lower velocities for other values of the series resistor. The increase in u_ϕ from $R_s=10$ Ω to $R_s=0.5$ Ω is consistent with the larger V_p expected across the plasma (although R_p indeed decreases with

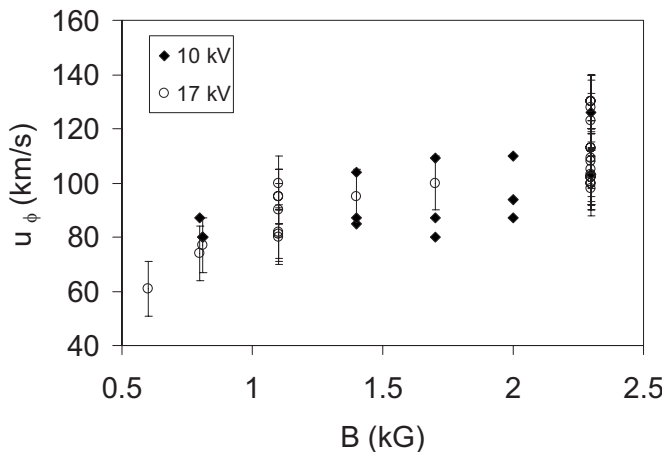


FIG. 5. Dependency of plasma rotation velocity on the magnetic field at the midplane for $B=0.23$ T, $R_m=7.5$, $R_s=2$ Ω , and $p=5$ mTorr. The absolute value of the applied voltage used is shown in the legend.

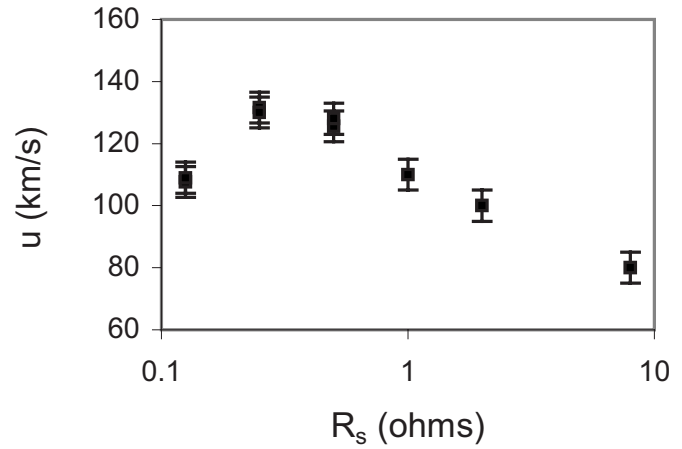


FIG. 6. Dependency of plasma rotation velocity at the midplane on the series resistor for $V_{\text{bank}}=-10$ kV, $B=0.21$ T, $R_m=6$, and $p=5$ mTorr.

decreasing R_s , as discussed later). Another more important observation is that u_ϕ actually drops as decreases from $R_s=0.5$ Ω to $R_s=0.125$ Ω , indicating a severe degradation in the plasma performance from a confinement standpoint. Finally, a mirror ratio scan was performed at an applied $V_{\text{bank}}=-14$ kV and a midplane magnetic field of $B=0.22$ T. Figure 7 documents that for all the discharges obtained, the maximum plasma rotation velocity is below a certain velocity v_{CIV} defined as

$$v_{\text{CIV}} = v_{\text{crit}} \times R_m^{1/2}, \quad (4)$$

where $v_{\text{crit}}=51$ km/s, which is the CIV in hydrogen. From Eqs. (3) and (4), it follows that $u_\phi^{\text{insulator}} < v_{\text{crit}}$. This suggests that what limits the rotation on MCX could be the CIV phenomenon occurring near the insulator, where the degree of ionization might be less than at the midplane and the neutrals are essentially stationary; hence, the ion velocity in the laboratory frame is equal to the ion velocity in the neutrals frame.

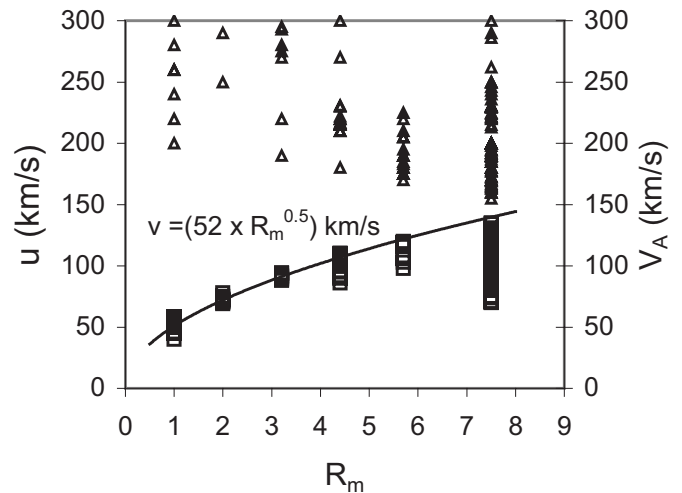


FIG. 7. Dependency of plasma rotation velocity at the midplane (square symbols, left vertical axis) on the mirror ratio for $V_{\text{bank}}=-14$ kV, $B=0.22$ T, $R_s=2$ Ω , and $p=5$ mTorr. The corresponding Alfvén velocity for each discharge is shown in triangle symbols, right vertical axis. The solid line corresponds to Eq. (4).

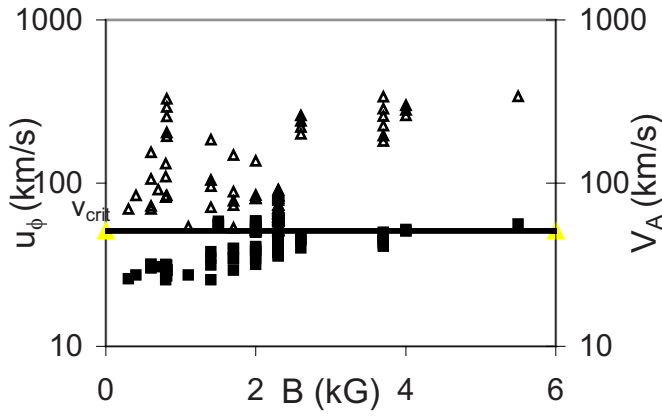


FIG. 8. (Color online) Dependency of plasma rotation velocity mapped at insulator using isorotation (square symbols, left vertical axis) on the magnetic field for $V_{\text{bank}} = -16$ kV, $R_m = 1-7.5$, $R_s = 2$ Ω , and $p = 5$ mTorr. The corresponding Alfvén velocity for each discharge (mapped to the insulator location) is shown in triangle symbols, right vertical axis.

To further test this hypothesis, the magnetic field scan was extended to the maximum achievable value of $B = 0.6$ T at the midplane, while lowering the mirror ratio accordingly. The rotation velocity measured at the midplane was then mapped to the insulator using Eq. (3). The results of this scan are shown in Fig. 8 and they indicate that over the entire range of MCX parameters, plasma rotation cannot exceed in a steady-state mode the v_{crit} velocity by more than 10%.

Also, plasma momentum confinement time has a decreasing trend as the rotation velocity mapped to the insulator location $u_{\phi}^{\text{insulator}}$ increases toward 51.4 km/s, irrespective of the mirror ratio used. This trend is documented in Fig. 9 for two mirror ratios, 7.5 and 1, respectively.

B. Trend of other plasma parameters near CIV limit

Other plasma parameters have also been monitored while attempting to increase the rotation speed at the optimal mirror ratio of $R_m = 7.5$. The experiments are performed by applying a large voltage from the capacitor bank, $V_{\text{bank}} = -14$ kV, and by lowering the series resistor R_s . Since

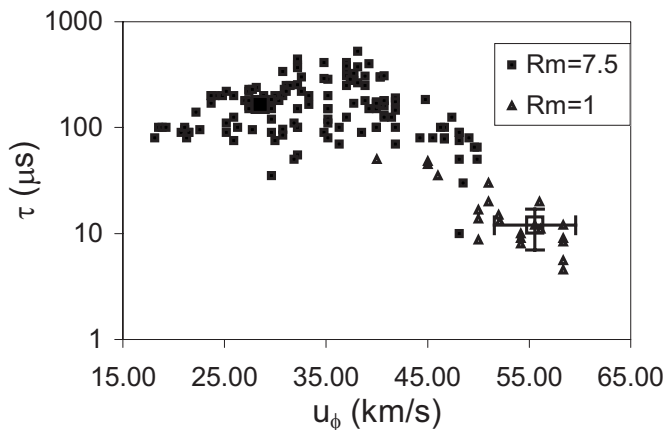


FIG. 9. Plasma momentum confinement time dependency on the rotation velocity for $R_m = 7.5$ (filled symbols) and $R_m = 1$ (open symbols).

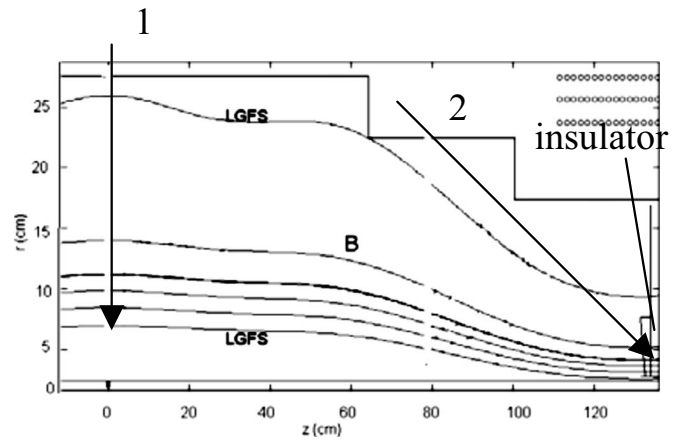


FIG. 10. Locations of collection optics for H_{α} radiation and the corresponding lines of sights: midplane (1) and insulator (2).

plasma voltage is a fraction of V_{bank} —see Eq. (2)—if the plasma resistance is constant, then it is expected that V_p will increase with decreasing R_s . However, as mentioned, the trend was that observed in Fig. 6. In this scan, other plasma parameters are also monitored: the ion temperature and the H_{α} emission. The ion temperature is measured from the Doppler broadening of the C^{2+} line with wavelength of $\lambda = 4647.42$ Å by looking radially into the plasma at the midplane. The sonic Mach number M_s will be found using the ion temperature measurement in combination with the voltage measurement and/or the Doppler shift of the same impurity line. A fiber optic cable (labeled “1” in Fig. 10) with a narrow (10 Å) bandpass filter monitors the H_{α} emission at the same location, and another identical fiber/filter combination (“2”) monitors the emission coming from the plasma-facing side of the end insulator (see Fig. 10).

Reducing the series resistor while keeping V_{bank} fixed leads to an increase in the plasma current I_p , i.e., the current between the inner electrode and the grounded vessel. While this is to be expected from the drop in R_s , the I_p rise is even greater since R_p also drops. This trend is seen in Fig. 11. In turn, this leads to an increase in the power dissipated into the plasma, $P = I_p \cdot V_p$. The effects of this power increase are documented in Fig. 12(a). It is found that the rotation veloc-

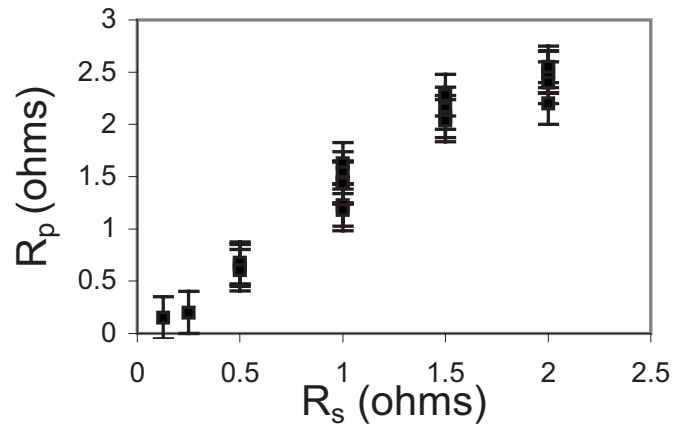


FIG. 11. Dependency of the plasma resistance R_p on the external series resistance R_s for $V_{\text{bank}} = -14$ kV, $R_m = 7.5$, and $p = 5$ mTorr.

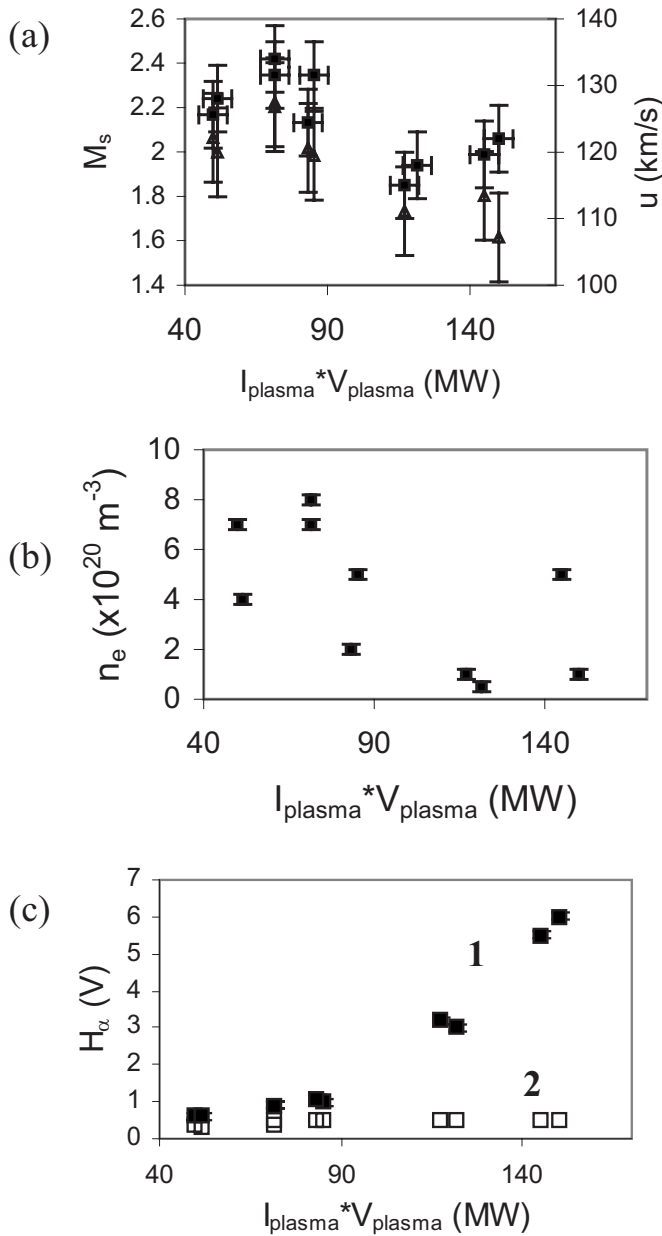


FIG. 12. (a) Plasma sonic Mach number (open triangles, left vertical axis) and rotation velocity (filled squares, right vertical axis) dependency on the plasma power while near the CIV limit. (b) Plasma density dependency on the plasma power while near the CIV limit. (c) Intensity of H_α signal at the midplane (filled symbols) and at the insulator (open symbols) while increasing plasma power near CIV limit.

ity drops about 10% and the ion temperature is almost constant within the experimental uncertainty, thus the sonic Mach number drops from around 2.2 to almost 1.6, while the dissipated power increases by almost 300%.

The plasma density at the time of maximum velocity also has a decreasing trend with increasing power, as shown in Fig. 12(b). However, the intensity of the H_α emission has a dramatic increase at the midplane of about 1200%, but almost no change at the insulator face—see Fig. 12(c). It is difficult to unravel what this increase means in terms of neutral density and electron temperature by simply using the H_α emission intensity measurement, but the difference in the trend of the signals at midplane compared to the insulator

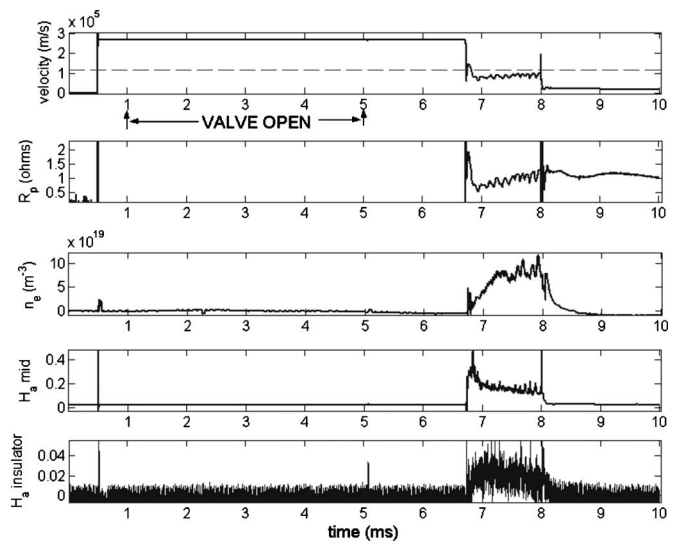


FIG. 13. Plasma rotation velocity (i.e., plasma voltage), plasma resistance R_p , density at the midplane, and the intensity of H_α signals at the midplane and insulator, respectively, in a discharge using a puff valve at the midplane. Rotation is below the CIV limit.

might suggest that neutrals at the midplane become more energetic as more power is dissipated into the plasma near this CIV boundary. The lack of means to measure the plasma density at the insulator and the observed decrease in plasma density at the midplane when $u_\phi \rightarrow v_{\text{CIV}}$ mean that an increase in plasma density at the insulator, as expected from an “increased ionization effect,”⁵ cannot be confirmed in MCX.

C. Experiments with puffed hydrogen gas

If the CIV phenomenon occurs at the plasma-insulator interface, this could be tested by transiently creating plasma at the midplane only. Thus, in an attempt to limit the plasma-insulator interaction during the discharge, the vacuum chamber was fitted with a gas-puffing valve (Parker-Hannifin 099-0167-900) at the midplane. The working assumption was that if the chamber could be filled in a time shorter than the time it takes the neutrals to expand all the way to the insulators, and ionization were to occur, the initial plasma would be rotating and confined away from the insulators. Transiently, one might observe super-CIV rotation. As representative numbers, the insulators are 1.3 m from the valve: the corresponding sonic time at standard temperature and pressure is about 1 ms. The ionization time is short, about $5 \mu\text{s}$. The fact that the H_α signals at the midplane and at the end insulator show no time lag between them is indicative of the fact that plasma might take about 4 ms to fill the chamber. However, the $\mathbf{E} \times \mathbf{B}$ rotation would be established quickly also, and thus a transient fast rotation could be possible.

The results of this campaign are summarized in Fig. 13. The voltage from the capacitor bank (-10 kV) is applied at $t=0.5$ ms. The valve is opened at $t=1$ ms and closed at $t=5$ ms. The breakdown occurs at $t \sim 6.7$ ms and the bank voltage is disconnected at $t=8$ ms. The puff valve had to be kept open for 4 ms in order to produce enough neutral density to initiate the discharge. Although this time is probably

less than the time a neutral puff would take to reach the insulators, the data show that the discharge obtained was very similar to those discharges when the chamber was pre-filled with hydrogen and the maximum plasma rotation speed was about 120 km/s. Moreover, the time dependence of the H_α line intensity as measured at the midplane and the end insulator shows that there is no time lag between the two signals. This indicates that the excitation of hydrogen atoms happens simultaneously at both locations.

D. Experiments with increased plasma length

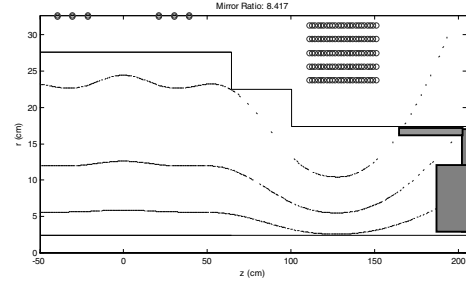
In the MCX experimental setup, increasing the separation between the insulators leads to several new considerations, some potentially favorable to experimental goals. Primarily, moving the insulators fans out the field lines, which intersect the insulator. This would presumably reduce coupling to the plasma. The reduced coupling could possibly affect any ionization phenomena, such as CIV. Thus, this is a worthwhile modification for our purposes. Second, moving the insulators could reduce the amount of recycled neutrals that penetrate into plasma, as conjectured from the theoretical work,²⁰ which indicates that neutral penetration from outside the flux conserving surfaces into the plasma can be much larger along the field lines (axial penetration) compared to the penetration across the field lines (perpendicular penetration). Finally, there could also be a breakdown of isorotation which could further help decouple any CIV-type mechanisms.

As part of the campaign to gain an understanding of and possibly mitigate the CIV-type phenomena, MCX was modified to a “long plasma” configuration. The two insulators were moved 0.5 m axially outward away from their original location at the mirror throat ($z = \pm 1.3$ m), so that the plasma-facing side of each of them was at $z = \pm 1.8$ m from the midplane—see Fig. 14(a). A Pyrex cylinder, of a diameter equal to that of the chamber at $z = \pm 1.8$ m, was inserted so that the entire plasma between the flux conserving surfaces was still ending on an insulating surface and not on the conductive wall. With that, the mirror geometry has also changed in the sense that for a mirror ratio of $R_m = 7.5$, the plasma cross section just in front of the insulator is actually equal to 0.12 m. Since the plasma can now be extended axially beyond the point of magnetic maximum, the magnetic flux conservation gives the ratio between the plasma cross section at the midplane (0.19 m) and at the insulator (0.12 m),

$$R_{\text{eff}} = \left(\frac{0.19}{0.12} \right)^2 = 2.5. \quad (5)$$

Measurements of the plasma rotation velocity were performed in a manner similar to the previous case when insulators were placed at the magnetic maximum using a pre-filled vacuum chamber. A typical result is shown in Fig. 14(b) (MCX090209-10). Rotation velocity has a distinctive feature now: in the beginning of the discharge, its value reaches about 85 km/s during a time interval of 100 μ s (corresponding to about three momentum confinement times). Later in the discharge, rotation drops and stabilizes to about

(a)



(b)

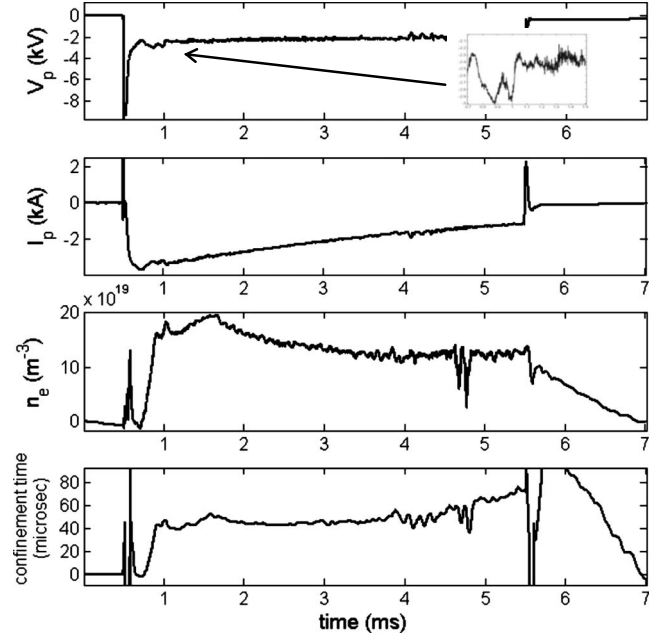


FIG. 14. (a) Quadrant view of the location of the plasma-facing side of the perpendicular insulator at $z = \pm 1.8$ m from the midplane (default location is $z = \pm 1.3$ m, at the magnetic maximum). Three magnetic field lines are shown: those corresponding to the two LGFS and the line at the junction of the perpendicular and parallel insulators. (b) Discharge representative for the plasma in the new insulator location configuration. The inset in the voltage trace shows the transient behavior between $|V_p| = 3$ kV (i.e., $u_\phi = 85$ km/s) and $|V_p| = 2.5$ kV (i.e., $u_\phi = 70$ km/s).

70 km/s. Mapping these two speeds to the location of the insulator using R_{eff} yields 57 and 46 km/s, respectively. While the former speed is slightly above the CIV velocity of 51.4 km/s, the latter one is below it. It can be concluded that these experiments show that CIV could be exceeded only for short periods of the discharge and only by a small fraction. Thus, plasma-neutral interaction at the new location of the insulator could still be responsible for the velocity limit observed.

To place these results in context, it is necessary to elaborate on the magnetic geometry and insulator placement of the “long plasma system.” In standard operation, all field lines inside the last closed flux surfaces intersect the axial insulator. In the present long configuration, the fanning out of the field lines means that the outer lines intersect the cylindrical vessel. This is why the Pyrex cylinder system was set up, to ensure that all field lines inside the last closed flux surfaces

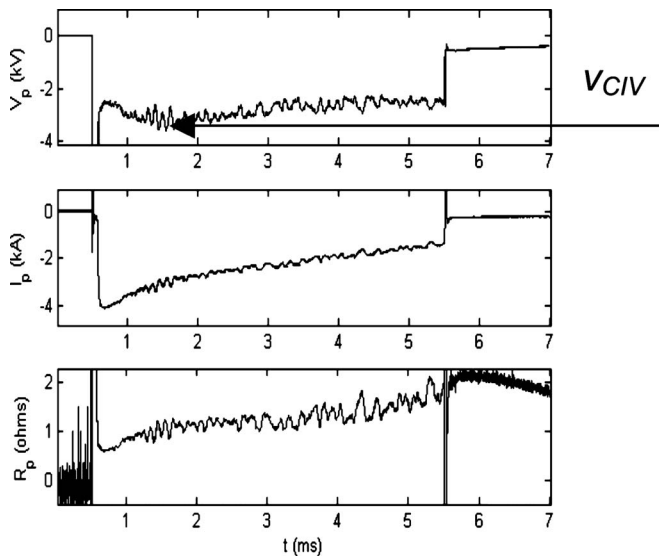


FIG. 15. Discharge representative for the helium plasma using the original insulator location configuration. Maximum rotation velocity is below the CIV limit in helium.

end on insulators. The cylinder is placed so that it presses against the Pyrex disk; the gap between the cylinder and the disk is minimized to a millimeter or less tolerance. Given the narrowness of this gap, all field lines within the gap are transverse to the gap and this setup ensures that all good lines end on insulators. As a final precaution, a cylindrical Mylar sheet was placed concentrically around the Pyrex. Some details on this set up are provided in the Appendix .

Earlier experiments to determine the effect of axial insulator placement on the discharge performance on MCX had been carried out by Lunsford.²¹ Three different axial positions for the insulator were tried: insulators at the mirror throat and insulators shifted 0.09 and 0.29 m outward from the mirror throat. There were several differences between these experiments and the present ones reported in this paper: (a) the present experiments have a larger maximum displacement than Lunsford's (0.50 and 0.29 m, respectively); (b) Lunsford's experiments were done using a different insulator than the one used in the current work; the main differences were that the older insulator had a smaller diameter for the grooved Macor piece (half of the current one) and the total path length along the surface of the Macor was smaller in the old insulator (by about a factor of 10; longer surface path being the motivation for the present insulator); and (c) in Lunsford's experiments, the whole insulator assembly (disk and alumina sleeve) was translated axially outward, as opposed to the present experiments where the alumina sleeve end was made to stay at the mirror throat (thus, in the old experiments, the metallic core was exposed by up to 0.29 m outside the mirror).

Lunsford's²¹ results for the rotation speeds measured were as follows: for fixed applied parameters and $R_m=7.8$, plasma rotation at the midplane was $u_\phi^{\text{midplane}}=86 \pm 2$ km/s when insulators were positioned at the mirror throat, 87 ± 3 km/s with insulators placed 0.09 m outside the mirror throat, and 83 ± 4 km/s with insulators 0.29 m outside the mirror throat. The overall inference from these

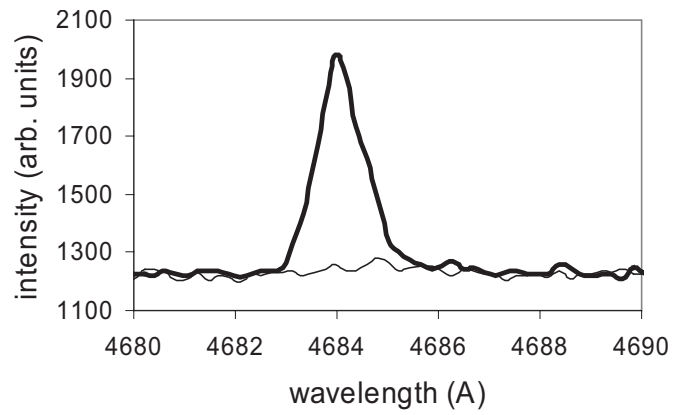


FIG. 16. Intensity of the He^+ line with wavelength of 4685.70 \AA at the time of maximum rotation velocity as measured at the midplane (thick line) and insulator (thin line).

results was that moving out the insulators did not change the rotation speed by much, a finding that does not bolster the ideas that motivated the experiment (as described at the beginning of this section). At the outermost insulator location of 0.29 m outside the mirror throat, the effective mirror ratio as defined by Eq. (5) was $R_{\text{eff}}=(0.21 \text{ m}/0.1 \text{ m})^2=4.4$. Compared to the mirror ratio of 7.8 at the mirror throat location, this corresponds to a “fanning out” of field lines by an area ratio of about 40%. Thus, it appears that the rotation speeds were not affected by the fanning out (at least for the limited scans conducted). For the effective mirror ratio of 4.4 at the outermost location, the CIV speed at midplane becomes $51.4 \times (4.4)^{1/2} \text{ km/s}=107 \text{ km/s}$. Hence, plasma rotation velocity as measured for that location, of 83 km/s, was also below the CIV limit for that location (and hence all locations) of the insulator position in Lunsford's experiments.

E. Experimental results from discharges in helium

Discharges were performed to investigate the predicted dependence of CIV on the neutral species mass and ionization potential by prefilling the chamber with helium as opposed to hydrogen. The experiments were done in a manner similar to those where hydrogen is used. The only difference is that now the spectrometer was set to monitor the plasma species He^+ ion line at 4685.7 \AA .

Typical discharges in helium, shown in Fig. 15, were similar to those in hydrogen. The maximum plasma rotation velocity measured at the midplane was $u_\phi=90$ km/s. Since the mirror ratio used was $R_m=6$, this velocity corresponds to $u_\phi^{\text{insulator}}=37$ km/s at the location of the insulator (mirror throat, $z=\pm 1.3 \text{ m}$). For helium neutrals to singly ionize via the critical velocity ionization phenomenon, the critical velocity in helium is $v_{\text{crit,He}}=35$ km/s. The Alfvén velocity was equal to 180 km/s, thus it did not constitute a limit in itself under those circumstances. Thus, the maximum plasma rotation was limited to a value consistent with the CIV limit at the insulator. Similar results were obtained earlier in MCX.²¹ However, at that time there were no interferometric measurements so v_A could not be determined.

As seen in Fig. 16, the most intense He^+ line (thick line)

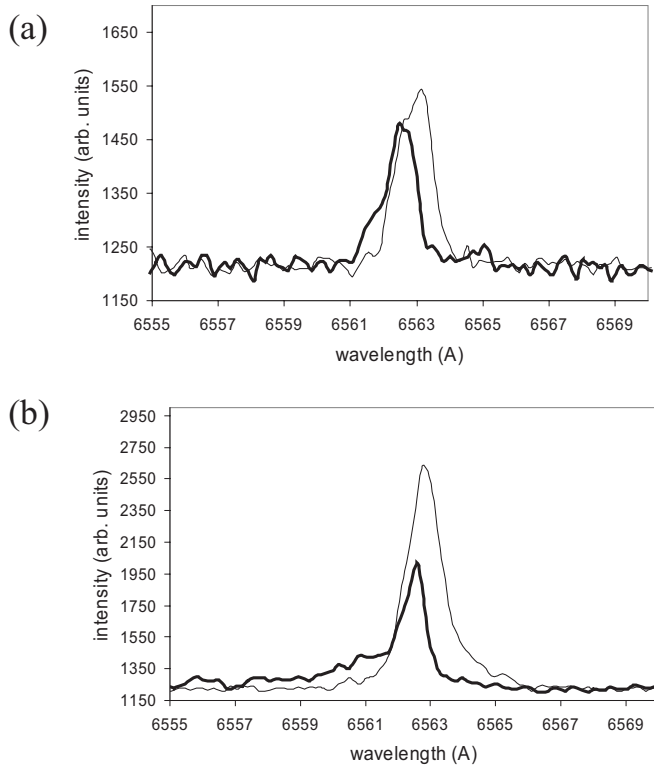


FIG. 17. (a) Intensity of the H_α line at the time of maximum rotation velocity in a helium discharge as measured at the midplane (thick line) and insulator (thin line) for low plasma power (16 MW) and rotation below CIV in helium. (b) Intensity of the H_α line at the time of maximum rotation velocity in a helium discharge as measured at the midplane (thick line) and insulator (thin line) for high plasma power (34 MW) and rotation 20% above CIV in helium.

was measured in a tangential view across the plasma at the midplane, being more than one order of magnitude larger than the same line emitted at the insulator (thin line). The Doppler shift corresponds to a rotation velocity of $u = 90 \pm 10$ km/s, consistent with the average value $u_\phi = V_p / (aB)$ of 90 km/s. The Doppler broadening yields an ion temperature of $T_i = 40$ eV, hence a sonic Mach number $M_s \sim 3$. These numbers are similar to those of a hydrogen plasma in MCX.

1. Penetration of helium plasma by impurity hydrogen

An interesting feature has been observed in helium discharges when attempting to increase the power input into the plasma by reducing the value of the series resistor R_s . The H_α line emitted from the plasma-facing side of the insulator was monitored and measured at the time of maximum plasma rotation velocity. Although no hydrogen was prefilled into the chamber, a small amount of H_α radiation was detected both at the insulator and at the midplane, as shown in Fig. 17(a), when the applied voltage was -10 kV and the series resistor was 2Ω . When the power input into the plasma was increased from 16 to 34 MW by using a 1Ω series resistor connected to a -10 kV biased capacitor bank, an increase of 400% was observed in the intensity of the H_α line at the end insulator—Fig. 17(b). The increase in the H_α

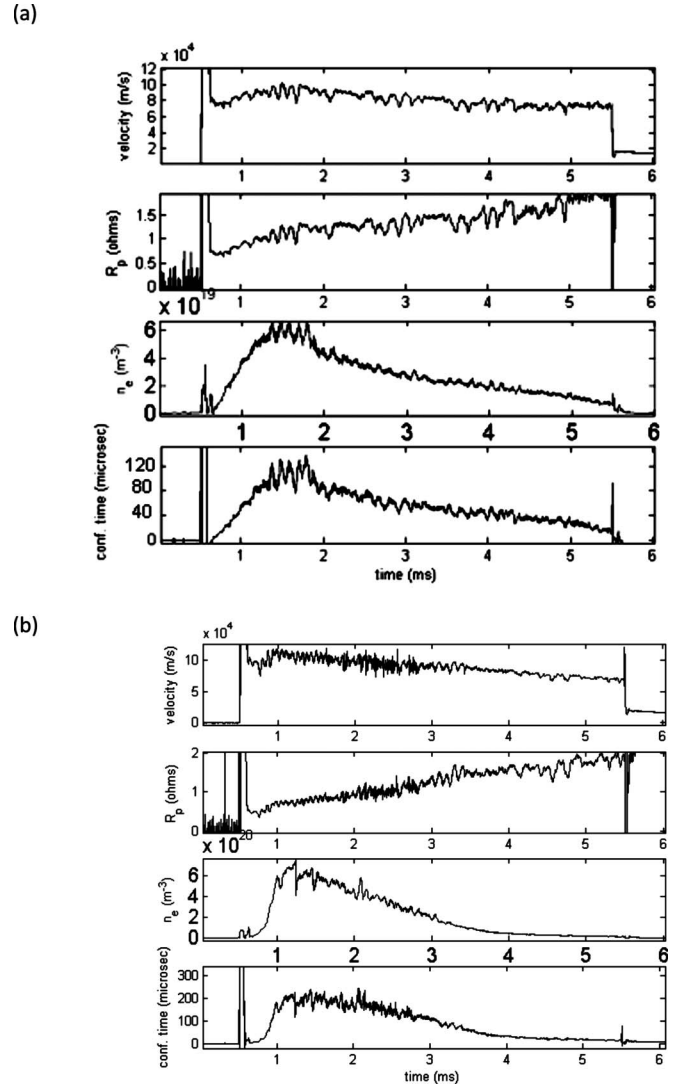


FIG. 18. (a) Plasma rotation velocity, plasma resistance, density at the midplane, and confinement time using helium at prefill pressure $p = 5$ mTorr and $V_{\text{bank}} = -10$ kV, $B = 0.23$ T, $R_m = 7.5$, and $R_s = 2 \Omega$, yielding low plasma power (16 MW). (b) Plasma rotation velocity, plasma resistance, density at the midplane, and confinement time using helium at prefill pressure $p = 5$ mTorr and $V_{\text{bank}} = -10$ kV, $B = 0.23$ T, $R_m = 7.5$, and $R_s = 1 \Omega$, yielding high plasma power (34 MW).

line at the midplane was only 200%. The increases in the intensities of the H_α and He^+ lines could indicate possible electron heating, consistent with earlier findings³ on the CIV process. A direct consequence of this heating could be the decrease in the neutral penetration depth, as seen from Eq. (8).

This suggests that hydrogen impurity atoms penetrate the plasma and remain mostly neutrals near the insulators, while at the midplane they could be ionized, hence the smaller increase in the H_α line intensity at the midplane. An increase in the plasma electron density—so measured by the interferometer at the midplane and shown in Figs. 18(a) and 18(b)—from 6×10^{19} to $7 \times 10^{20} \text{ m}^{-3}$ is detected under these circumstances. It is also likely that doubling the power leads to increased ionization within the helium population so that the fraction of doubly ionized ions (ionization energy of 54.4 eV) increases, thus releasing more electrons into the

plasma. Nonetheless, the value of the helium prefill pressure was not changed when doubling the power input into the plasma, and an increase of more than one order of magnitude in the density is observed. This increase can be partially attributed to hydrogen impurities penetrating the helium plasma and ionizing at the midplane. It is quite likely that the hydrogen influx came from water desorbed during plasma shots from the insulator surface and elsewhere; in particular, the residual gas analyzer measurements showed water to be the most prominent impurity before prefill or gas puff shots (at base vacuum levels of the order of 10^{-7} Torr). The confinement time in Fig. 18(a) was calculated, assuming that the plasma is 100% helium, and in Fig. 18(b), assuming that 10% of the density is helium and 90% is hydrogen.

With more input power, the peak value of the rotation velocity at the midplane reaches transiently 115 km/s, meaning 42 km/s at the insulator. This is approximately 20% more than v_{crit} in helium. Exceeding the CIV in helium by such amount can be explained by the fact that ions now move through a mixture of helium atoms and hydrogen atoms near the insulator. Since the critical velocity in hydrogen is 45% larger than in helium, it can allow a plasma mixture consisting of singly ionized helium ions, alpha particles, and protons to rotate faster when encountering the helium and hydrogen atoms than in the case of helium ions moving through helium atoms. A velocity limit equal to the combination of the critical ionization velocities of the component species in a multispecies plasma has been documented in the past.²²

IV. DISCUSSION

In the MCX, plasma rotation is commenced and maintained by coupling the plasma to an external source, the capacitor bank, which is responsible both for the initial plasma breakdown and the subsequent rotation. In general MCX operation, for typical capacitor bank settings, the plasma attains a large Reynolds number, that is to say, the rotation rate can be to 40 times larger than the plasma momentum confinement rate. MHD instability growth rates are expected to be on the order of the rotation rate, and thus the plasma momentum is conserved over many instability times. The stored charge in the external bank is about 20 times larger than the plasma stored charge Q_p , and thus the MCX plasma attains a quasistatic equilibrium state over several confinement times. In this state, the basic MHD force balance equation of a stationary, axisymmetric, magnetized plasma rotating in the presence of ion-neutral collisions can be written as

$$\rho(u \cdot \nabla)u + \rho u v_{\text{cx}} = \mathbf{j} \times \mathbf{B} - \nabla p, \quad (6)$$

where v_{cx} is the charge-exchange rate due to ion-neutral collisions and, for simplicity, the neutrals are assumed to be at rest in the laboratory frame. These collisions are responsible for the drag of the plasma and the reduction in the rotation speed through momentum transfer between ions and neutrals. In the 0-D model of MCX documented previously,¹⁸ the charge-exchange time v_{cx}^{-1} was equated to the plasma momentum confinement time τ to infer the ionization fraction in the plasma (more than 99% ionized).

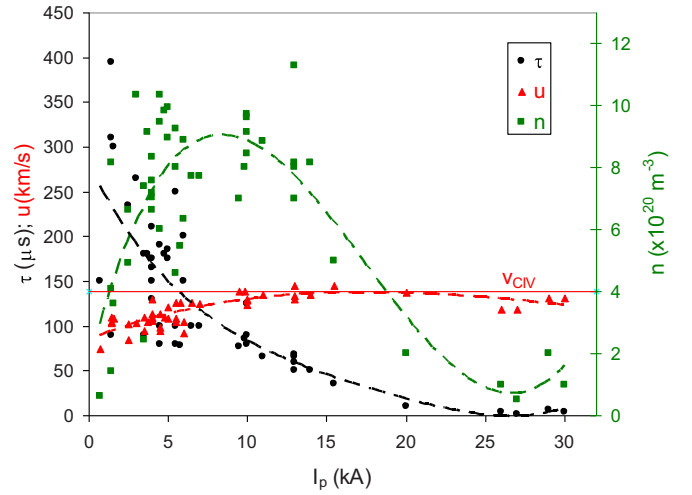


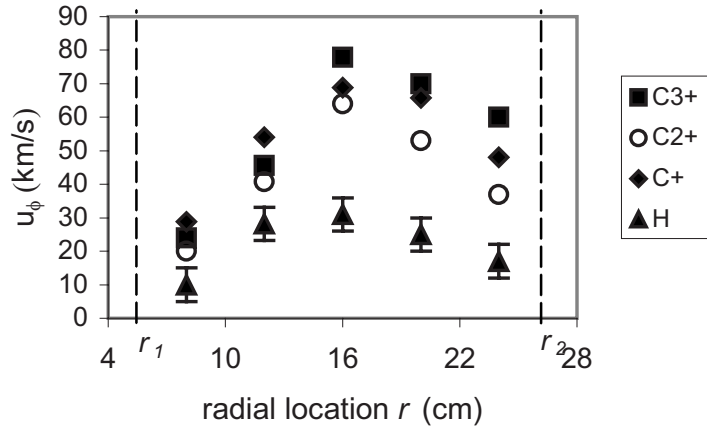
FIG. 19. (Color online) Dependency of plasma rotation velocity, confinement time (both left vertical axis), and density (right vertical axis) recorded at the time of maximum velocity on the absolute value of the plasma current for $B=0.23$ T and $R_m=7.5$.

Modeling MCX as a cylindrical system in (r, ϕ, z) coordinates, with z along the axis of symmetry, azimuthal plasma rotation, $\mathbf{u}=(0, u_\phi, 0)$, and ignoring the mirror field, for simplicity, the azimuthal component of the momentum balance equation becomes

$$\frac{\rho u_\phi}{\tau} = j_r B_z \quad (7)$$

where τ is the charge-exchange time or, in general, could represent some other momentum loss mechanism (such as classical viscosity or MHD turbulence losses). Equation (7) shows that a radial current j_r is necessary so that net momentum loss via ion-neutral collisions can be balanced by the $\mathbf{j} \times \mathbf{B}$ force. The radial current is proportional to I_p , the current into the plasma capacitor. From Eq. (7), we note that, for fixed magnetic field, plasma velocity u_ϕ could be increased by increasing I_p (assuming fixed plasma density and the same plasma conditions resulting in the same confinement time). I_p , in turn, could be increased by ramping up the externally applied voltage since $I_p = V_{\text{bank}} / (R_s + R_p)$. We summarize the results of a campaign to force more current through the plasma in an effort to increase the flow speed in Fig. 19. Here, as a function of increasing I_p , we show all data points for the maximum speed attained, maximum density at the time of the maximum speed, and the confinement time at the time of maximum speed. The dashed lines are best fits of the data. There is a small increase in the speed for low I_p but this saturates to below v_{CIV} for $|I_p| > 12$ kA. In fact, for $2.2 \text{ kA} < |I_p| < 12 \text{ kA}$, a fivefold increase in the plasma current, the rotation velocity increases by only about 50%. This small increase in the velocity can be understood in the context of Eq. (7) by noting the trends in the plasma density n and confinement time τ : in that same I_p range, the density increases by about a factor of 4 and confinement time decreases by about 35%. Thus, the increase in the rotation velocity expected from increasing the current is not realized; instead, the extra momentum input from the $\mathbf{j} \times \mathbf{B}$ force

(a)



(b)

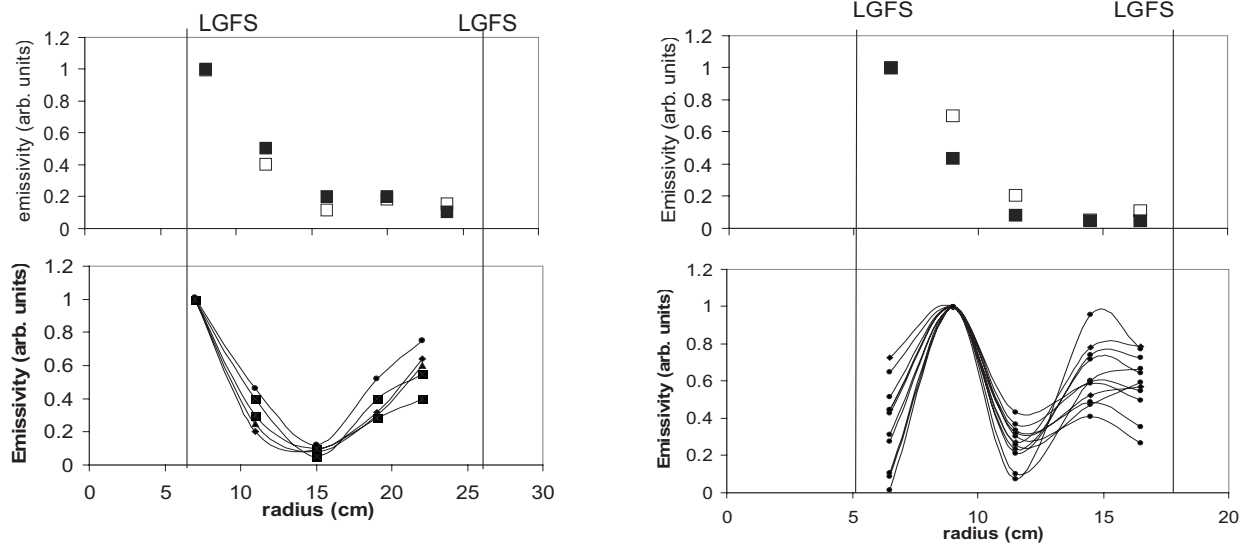


FIG. 20. (a) Radial profile of plasma rotation velocity as measured from the Doppler shift of spectral lines emitted by C impurity ions and the H_α line. The maximum relative velocity between C^{3+} and neutrals is 48 km/s at $r=16$ cm. (b) Left: the relative intensity of C^{3+} spectral line (upper) and H_α line (lower) at the midplane. Right: the relative intensity of C^{3+} spectral line (upper) and H_α line (lower) at $z=0.85$ m away from the midplane.

manifests mostly as an increase in the plasma density and a (relatively smaller percentage) lowering of the confinement time.

When plasma reaches rotation velocities at the midplane around $u_\phi \approx 139$ km/s, further increasing the absolute value of the current $|I_p|$ beyond 15 kA does not further increase the rotation, which remains at this value or slightly below it. For these currents, the plasma density actually drops by a large factor; the major drop is in the confinement time. This trend can be interpreted as that the plasma is experiencing a velocity limit and attempts to push the plasma through this limit lead to a large overall degradation of the plasma parameters.

An interesting feature observed in spectroscopic measurements at the midplane ($z=0$) is that the relative velocity between the ions and neutrals is less than 51.4 km/s at all radial locations: in particular, this velocity difference is less than the critical velocity $v_{crit}=51.4$ km/s. This is the case for all discharges considered. As an example, we show in Fig. 20(a) spectroscopic measurements at the midplane ($z=0$) of the rotation profiles of plasma and neutrals: while both profiles are parabolic-type, the neutral speeds are lower

than the ions. This is to be expected, since, as the ions rotate according to the $\mathbf{E} \times \mathbf{B}$ drift, ion-neutral drag can be expected to bring up the neutral speed to that of the plasma. A theoretical analysis of the drag physics could yield the differential speed between the two species. However, there is not sufficient diagnostic information to compare the analysis to the experimental observations. For the present purposes, we simply note this interesting feature and acknowledge its possibly coincidental nature.

Line intensity measurements of hydrogen neutrals suggest that neutrals are hollowed out in the plasma core; in all discharges analyzed, the plasma core seems depleted of neutrals. This can be seen in Fig. 20(b): in the left hand panels of Fig. 20(b), we show the intensity of the C^{3+} line and the H_α line at $z=0$. The H_α line intensity in the plasma core ($r=16$ cm) is more than one order of magnitude smaller than at the plasma edges ($r_1=0.06$ m and $r_2=0.26$ m, respectively), in agreement with the 0-D model.⁹ Away from the midplane ($z=0.85$ m), the spectroscopic Doppler shifts show similarity to those at the midplane in that the relative velocity between impurity ions and neutrals is smaller than

the critical velocity; the radial profile of the neutrals, however, can be different from the midplane, as seen the bottom right hand panel of Fig. 20(b), which suggests greater neutral penetration (the C^{3+} profile, upper right hand panel, is similar to the midplane). In the absence of information on the electron temperature profile, information on the neutral density inferred from H_α line intensity is somewhat of a conjecture. To compensate for the fact that only five spectral chords could be set up, many discharges were taken under the same conditions and the shot-to-shot reproducibility is shown.

Neutral penetration depths into plasma are on the order of the mean free path of a neutral from charge-exchange with plasma ions and electron impact ionization,²³ i.e., $\lambda_{\text{mfp}} = (\lambda_{\text{cx}}^{-1} + \lambda_{\text{ionize}}^{-1})^{-1}$, where $\lambda_{\text{cx}} = 1/(n\sigma_{\text{cx}})$ and $\lambda_{\text{ionize}} = u_{\text{rel}}/(n\sigma_{\text{ionize}}v_{\text{th,e}})$. Using as the relative velocity $u_{\text{rel}} = 51.4$ km/s, $n = 1 \times 10^{20}$ m⁻³, the charge-exchange cross section $\sigma_{\text{cx}} = 5 \times 10^{-19}$ m², $T_e = 10$ eV, $T_i = 40$ eV, and

$$\sigma_{\text{ion}}v_e = \frac{2 \times 10^{-13}}{6 + T_e/13.6} \left(\frac{T_e}{13.6} \right) \exp\left(\frac{-13.6}{T_e} \right), \quad (8)$$

the mean free path of neutrals is approximately $\lambda_{\text{mfp}} \approx 0.02$ m. This is small compared to the plasma cross section at the midplane, namely, $\lambda_{\text{mfp}}/a = 1/10$; near the insulators, however, the plasma cross section becomes as small as $a_{\text{ins}} = 0.065$ m, hence $\lambda_{\text{mfp}}/a_{\text{ins}} = 1/3.25$. In addition, with centrifugal confinement, the plasma density near the insulators is expected to be significantly lower; thus, neutral penetration into plasma near the insulators is significant and neutral-ion interaction can impact the plasma more significantly at the insulators than at the midplane. An increase in the electron temperature (as suggested by the increase in the H_α and He^+ lines intensities near CIV) could result in the decrease in the neutral penetration depth. For the range of plasma density and ion temperature values we measure, the charge-exchange mean free path is smaller than the electron impact ionization mean free path as long as $T_e < 9$ eV. For higher electron temperatures, the charge-exchange mean free path becomes larger than the electron impact ionization one.

V. SUMMARY

Experiments on plasma rotation on MCX have indicated an upper bound on the maximum rotation speed. This upper bound is distinct from the Alfvén speed limit reported previously.² It was suggested in earlier work on this topic¹⁹ that this upper bound on the speed could be the “CIV,” originally proposed by Alfvén; this phenomenon has to do with the enhanced ionization near surfaces if the nearby $\mathbf{E} \times \mathbf{B}$ kinetic energy exceeds the ionization potential of the species. For hydrogen, this speed is 51.4 km/s. Assuming that this speed limit is operative at the insulators and that $\mathbf{E} \times \mathbf{B}$ rotation in systems such as MCX is “rigid rotor” per field line (which is the case for ideal MHD conditions), 51.4 km/s at the insulators would translate to $51.4 \times R_m^{1/2}$ km/s at the midplane (with R_m being the mirror ratio). The results of a previous experimental campaign on MCX (Ref. 2) to increase the rotation speed showed an upper bound at the midplane below the CIV speed (as just defined). In the present

paper, we report on various methods that were tried to attain high velocities in MCX and report that, for all the methods tried, this upper bound was not exceeded. All MCX results to date, from the previous campaign² and from the present paper, can be summarized by the condition $u_\phi^{\text{max}} \leq v_{\text{crit}} \times R_m^{1/2}$, where u_ϕ^{max} is the measured speed at the midplane and $v_{\text{crit}} = 51.4$ km/s for hydrogen plasma and 35 km/s for helium plasma (for $R_m = 7.5$, this corresponds to $u_\phi^{\text{max}} < 139$ km/s for hydrogen.) In all discharges studied here, the Alfvén velocity was always larger than $v_{\text{crit}} \times R_m^{1/2}$, ruling out the ideal MHD Alfvén Mach number limitation reported earlier.² Other previous experiments^{19,21} did not distinguish between the CIV phenomenon and the Alfvén Mach number limit $M_A \leq 1$.

In the present campaign, direct attempts to increase the rotation speed in the $R_m = 7.5$ configuration to above 139 km/s at the midplane, by increasing the applied voltage and/or lowering the series resistor in the external electric circuit, were not successful (within the range of externally applied parameters currently available at MCX). Instead, a large increase in the plasma density and/or a degradation of the plasma confinement time was seen as the applied parameters were chosen such as to place a larger voltage across the plasma. More intense radiation from neutral hydrogen in both hydrogen or helium plasmas was observed for fixed prefll pressure, pointing to enhanced particle recirculation from the chamber walls.

Operating the system in a longer plasma configuration, by placing the insulators further from mirror throats, in an attempt to “decouple” the plasma from the insulator, has been also proven unsuccessful insofar as reaching speeds higher than the critical speed: experiments done earlier,²¹ utilizing modest increases in system length, showed almost no change in the highest speed obtained; in the present campaign, an experimental setup with a longer length and significant field expansion showed a decrease in the maximum speed, to just at or under the critical speed as defined above; the latter result, while indicative, is tentative since a relatively simple configuration of end insulators (described in Sec. III D) was used and improvements in insulator design are under consideration. Experiments with a puff valve in standard configuration (insulators at the mirror throats) also indicated plasma rotation limited by the critical speed.

APPENDIX: DETAILS OF END INSULATOR PLACEMENT AT THE ENDS OF THE VACUUM CHAMBER

In the text, we discussed placements of the nested Pyrex and Mylar cylinders to effect appropriate field line terminations for the long plasma system experiments. In this appendix, we provide some more details on this setup. While the setup described in the text ensures that all “good lines” end on insulators, the radial shortness of the gap presents the possibility that the resistance across the gap, even though cross field and thus of high resistivity, could allow some electrical connection. As discussed, to protect against this possibility, a nested cylinder of Mylar with length of 10 cm was placed concentrically over the Pyrex cylinder. Thus, any

discharge across the gap would still not directly contact the grounded vessel; in addition, any continuation of such a discharge would have to be along the Mylar and across the lines, a relatively high resistance path. Experiments were then conducted in this “long” mode over hundreds of discharges. Over the course of this experimental campaign, there was considerable carbon deposition on the Mylar. In addition, there was evidence of some arcing. In previous MCX experiments^{15–18,21} with various different insulator systems, there has always been strong carbon deposition without any accompanying degradation of the system, and arcs have been found to be isolated events. In this sense, the present experimental standards are consistent with previous experimental standards on MCX, and the results obtained in this campaign can be viewed with some confidence. That said, it must be added that the conclusions drawn from the present experimental results are of considerable import, in particular, implying that MCX maximum speeds still seem to be limited by the CIV speed. Given the importance of the implication, that fanning out of field lines does not seem to be helpful, the results are viewed as strongly suggestive only. A future experiment is being considered where the gap can be eliminated (which would obviate the Mylar).

¹A. B. Hassam, Phys. Plasmas **B** **4**, 485 (1992).

²C. Teodorescu, R. Clary, R. F. Ellis, A. B. Hassam, R. Lunsford, I. Uzun-Kaymak, and W. C. Young, Phys. Plasmas **15**, 042504 (2008).

³N. Brenning, Space Sci. Rev. **59**, 209 (1992).

⁴S. T. Lai, Rev. Geophys. **39**, 471, doi:10.1029/2000RG000087 (2001).

⁵H. Alfvén, *Cosmical Electrodynamics* (Clarendon, Oxford, 1950), pp. 50–85.

⁶U. V. Fahlson, Phys. Fluids **4**, 123 (1961).

⁷B. Angerth, L. Block, U. Fahlson, and K. Soop, Nucl. Fusion **1**, 39 (1962).

⁸J. Bergstrom, S. Holmberg, and B. Lehnert, *Proceedings of the Plasma Physics and Controlled Nuclear Fusion Research*, Culham, 1965 (IAEA, Vienna, 1966), Vol. I, pp. 341–356.

⁹B. Lehnert, Phys. Fluids **9**, 774 (1966).

¹⁰B. Lehnert, J. Bergstrom, and S. Holmberg, Nucl. Fusion **6**, 231 (1966).

¹¹L. Danielsson, Phys. Fluids **13**, 2288 (1970).

¹²A. Piel, E. Mobius, and G. Himmel, “The origin of turbulent heating in a critical velocity rotating plasma,” Report No. 78-M2-037 (Institut für Experimentalphysik II der Ruhr-Universität Bochum, 1978).

¹³N. Brenning, Phys. Fluids **28**, 3424 (1985).

¹⁴G. F. Abdrashitov, A. Beloborodov, V. Volosov, V. Kubarev, Yu. Popov, and Yu. Yudin, Nucl. Fusion **31**, 1275 (1991).

¹⁵J. Ghosh, R. C. Elton, H. R. Griem, A. Case, R. Ellis, A. B. Hassam, S. Messer, and C. Teodorescu, Phys. Plasmas **11**, 3813 (2004).

¹⁶J. Ghosh, R. C. Elton, H. R. Griem, A. Case, A. W. DeSilva, R. F. Ellis, A. Hassam, R. Lunsford, and C. Teodorescu, Phys. Plasmas **13**, 022503 (2006).

¹⁷R. F. Ellis, A. Case, R. Elton, J. Ghosh, H. Griem, A. Hassam, R. Lunsford, S. Messer, and C. Teodorescu, Phys. Plasmas **12**, 055704 (2005).

¹⁸C. Teodorescu, R. F. Ellis, A. Case, C. Cothran, A. Hassam, R. Lunsford, and S. Messer, Phys. Plasmas **12**, 062106 (2005).

¹⁹B. Lehnert, Nucl. Fusion **11**, 485 (1971).

²⁰S. Ng and A. B. Hassam, Phys. Plasmas **14**, 102508 (2007).

²¹R. Lunsford, Ph.D. thesis, University of Maryland, 2006.

²²I. Axxas, Astrophys. Space Sci. **55**, 139 (1978).

²³R. J. Goldston and P. H. Rutherford, *Introduction to Plasma Physics* (IOP, Philadelphia, 1997), pp. 151–160.